Dynamic Monte Carlo Simulation for Highly Efficient Polymer Blend Photovoltaics

8 AUTHORS, INCLUDING:

Qikai Li
Tsinghua University
46 PUBLICATIONS **1,141** CITATIONS

Xiaowei Zhan
Chinese Academy of Sciences
195 PUBLICATIONS **8,669** CITATIONS

Zhigang Shuai
Tsinghua University
319 PUBLICATIONS **10,090** CITATIONS

Alison B. Walker
University of Bath
48 PUBLICATIONS **1,758** CITATIONS

Dynamic Monte Carlo Simulation for Highly Efficient Polymer Blend Photovoltaics

**Lingyi Meng,[†] Yuan Shang,[†] Qikai Li,[†] Yongfang Li,[†] Xiaowei Zhan,*,[†] Zhigang Shuai,*,[†,‡]
Robin G. E. Kimber,[§] and Alison B. Walker*,[§]**

*Key Laboratory of Organic Solids, Beijing National Laboratory for Molecular Science (BNLMS),
Institute of Chemistry, Chinese Academy of Sciences, 100190 Beijing, China, Department of Chemistry,
Tsinghua University, 100084 Beijing, China, and Department of Physics, University of Bath,
Bath BA2 7AY, United Kingdom*

We developed a model system for blend polymers with electron-donating and -accepting compounds. It is found that the optimal energy conversion efficiency can be achieved when the feature size is around 10 nm. The first reaction method is used to describe the key processes (e.g., the generation, the diffusion, the dissociation at the interface for the excitons, the drift, the injection from the electrodes, and the collection by the electrodes for the charge carries) in the organic solar cell by the dynamic Monte Carlo simulation. Our simulations indicate that a 5% power conversion efficiency (PCE) is reachable with an optimum combination of charge mobility and morphology. The parameters used in this model study correspond to a blend of novel polymers (bis(thienylenevinylene)-substituted polythiophene and poly(perylene diimide-*alt*-dithienothiophene)), which features a broad absorption and a high mobility. The *I*−*V* curves are well-reproduced by our simulations, and the PCE for the polymer blend can reach up to 2.2%, which is higher than the experimental value (>1%), one of the best available experimental results up to now for the all-polymer solar cells. In addition, the dependency of PCE on the charge mobility and the material structure are also investigated.

1. Introduction

Organic polymer solar cells based on the bulk heterojunction structure have attracted great interest in recent years due to their potential application for low cost, ease of fabrication, mechanical flexibility, and light weight.[1−5] However, the power conversion efficiencies of organic cells are still generally too low to satisfy the requirement of commercial exploitation. Searching new materials with strong optical absorption, efficient charge separation, and migration is essential to improve the power conversion efficiency. It has been demonstrated experimentally that through controlling the nanostructure formed by electron-donating and -accepting moieties, the efficiency can be greatly increased.[6] Developing a computational approach for modeling the bulk heterojunction can be of help for the design of rational materials.

Recently, two new conjugated polymers (poly(perylene diimide-*alt*-dithienothiophene)[6] (type 1) and bis(thienylenevinylene)-substituted polythiophene[7] (type 2)) have been synthesized as shown in Figure 1, and they have been fabricated as an all-polymer organic solar cell that exhibits strong absorption throughout the visible and extending into the near-IR spectrum.[6] These two novel polymers also display relatively high charge mobility (electron mobility of type 1 is 1.3×10^{-2} cm^2 V^{-1} s^{-1}, and hole mobility of type 2 is $\sim 10^{-4}-10^{-3}$ cm^2 V^{-1} s^{-1}). The power conversion is found to be >1%.

Previous theoretical descriptions, including the continuum description of organic photovoltaic (OPV) devices (or the Poisson equation method)[8] and the dynamical Monte Carlo model with the first reaction method (FRM),[9,10] have been proposed. Watkins et al.[9] first developed a dynamical Monte
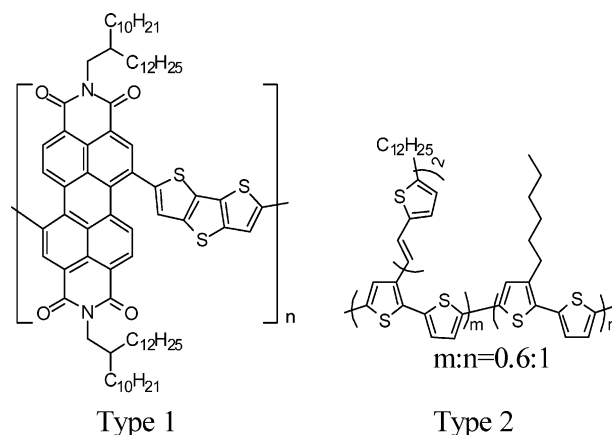

Figure 1. The chemical structures of poly(perylene diimide-*alt*-dithienothiophene) type 1 and bis(thienylenevinylene)-substituted polythiophene type 2.[6,7]

Carlo model to examine the dependency of short-circuit internal quantum efficiency (IQE) on the scale of phase separation in morphology. This model focuses on the IQE, but not for the *I*−*V* curve, and several important characteristics for an organic solar cell, including short-circuit current, open-circuit voltage, and fill factor, have been completely ignored. To improve the description of charge behavior, Marsh et al. designed a model including dark injection at the electrodes; however, the exciton creation, diffusion, and dissociation have been ignored in their model; thus, only charge transport in the organic nanostructures is considered.[10] In this work, we take all the microscopic photovoltaic processes, including both exciton and charge dynamics, occurring in a polymer blend device into account to obtain the absolute power conversion efficiency in OPV devices.

These processes are as follows: (i) Excitons are generated by the absorbed photons. (ii) Part of the excitons migrates to

* Corresponding author. E-mails: (Z.S.) zgshuai@tsinghua.edu.cn; (A.B.W.) a.b.walker@bath.ac.uk.
[†] BNLMS.
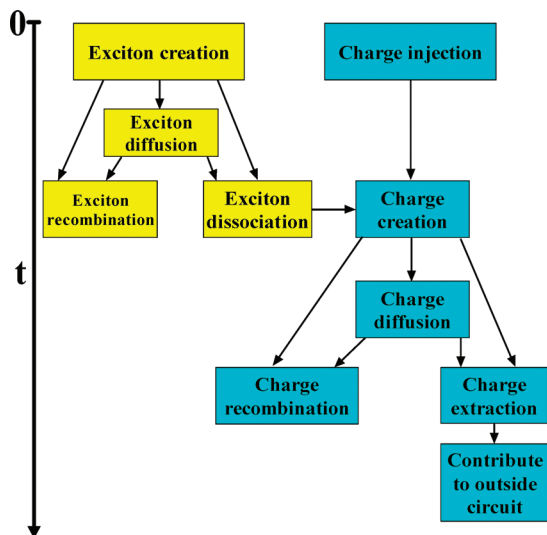[‡] Tsinghua University.
[§] University of Bath.

MC Simulation for Polymer Blend Photovoltaics

J. Phys. Chem. B, Vol. 114, No. 1, 2010 **37**

Figure 2. Scheme of the simulation processes, including dark current, photocurrent, exciton, and charge dynamics.
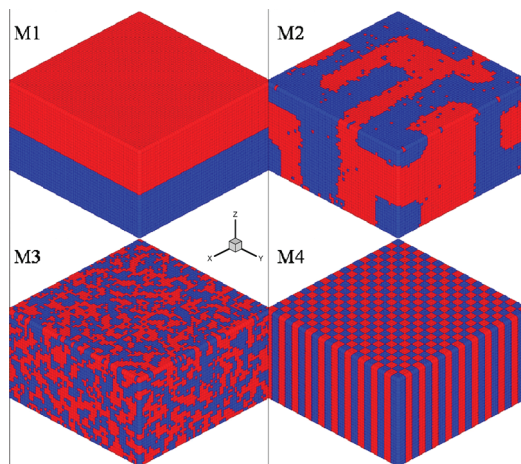

Figure 3. Typical morphologies with different scales of phase separation, M1 for the bilayer, M2 and M3 for the blend generated by using the Ising model, and M4 for the checkered structure. The electron and hole conductors are colored with red and blue, respectively.

the interface between the electron-donating and the electron-accepting domains to dissociate into electrons and holes before recombination. (iii) After the dissociation, an interfacially bound charge pair will be formed and is subject to the competition between the geminate recombination and the separation to be of free charges. (iv) Free charges will diffuse due to the density gradient, and the drift will be driven by the built-in field from the difference between the electrode work functions and the externally applied voltage. (v) Charge collection at the electrode, in which the free charges could meet an opposite charge at the interface to form a bound pair that will nongeminately recombine to disappear. Those free charges successfully approaching the electrodes could be extracted and contribute to the outside circle current. To permit a full treatment of the $I-V$ performance of devices, the thermionic injection of carriers from the electrodes must be integrated into the algorithm.[10-14] We give a scheme of the simulation processes in Figure 2.

Thus, we present here an integrated dynamical Monte Carlo model that includes both the dark current mechanism[10] and the photocurrent as well as a complete description of exciton behavior.[9] We apply this MC approach to investigate the morphology and the carrier mobility dependence of the polymer blend (types 1 and 2) to offer guidance to the ongoing experiment work and to give an estimate for the maximum power conversion efficiency at optimal condition for such system.

2. Model and Computational Approach

In the model system, the lattice is of the $60 \times 60 \times 30$ sites in the x, y, and z directions, respectively, and a lattice constant (a_0) of 3 nm is used (in consideration of the XRD datum for POTVT[15]). A single occupancy of lattices for any particle is imposed, and the system temperature, T, is fixed at 298 K. The electrodes (not shown in Figure 3) are parallel to the $x-y$ plane located at $z = 0$ and $z = 90$ nm. Periodic boundary conditions are applied in both the x and y directions. In the experiment of absorption measurement, the thickness of the solar cell film is normally around 100 nm. We can obtain a measure of the characteristic domain size, a, in these blends from the ratio of interfacial area, A, to the total blend volume, V, $a = 3V/A$. The cutoff value, R_c, in calculating the Coulombic interaction is 15 nm, which is close to the thermal capture radius.[10] The dielectric constant (ε) of the polymers is set as 3.5.

To obtain the optimized nanostructure with maximum power conversion efficiency, a series of blend morphologies (e.g., M2 and M3 as shown in Figure 3) with varying scales of phase separation must first be prepared by using the Ising model.[9] In the Ising model, the spin up and down correspond to the donor and acceptor phases, respectively, and the Hamiltonian for the energy contributed by site i is:

$$\varepsilon_i = -\frac{J}{2} \sum_j \left(\delta_{s_i,s_j} - 1 \right) \tag{1}$$

where δ_{s_i,s_j} is the delta function, and s_i and s_j are the spins occupying sites i and j. The summation over j includes all first- and second-nearest neighbors, and the energetic interaction is inversely proportional to the distance between neighboring sites i and j (the energetic contribution is scaled by a factor of $1/\sqrt{2}$ for the second-nearest neighbors). To obtain a series of morphologies with different phase interpenetrations, we need to decide the appropriate initial configuration and the corresponding interaction energy, J. In our simulation, the initial morphology with minimal phase separation is chosen, and the interaction energy, J, is set as $+1.0\ k_BT$. To relax the system to an energetically favorable state, the neighboring pairs of sites are chosen randomly in the system, and then the acceptance probability for an attempt to swap the site spins is calculated as

$$P(\Delta\varepsilon) = \frac{\exp(-\Delta\varepsilon/(k_BT))}{1 + \exp(-\Delta\varepsilon/(k_BT))} \tag{2}$$

where the $\Delta\varepsilon$ is the energy change in the system caused by swapping the site spins. After a large number of attempted spin swappings, a desired morphology series with varying scales of phase separation can be generated and stored for later use.

Bilayer morphology (M1 as shown in Figure 3) and an optimal checkered structure[9,16] (M4 as shown in Figure 3) are also chosen in the simulations as a comparison.

Three types of mobile particles (electrons, holes, and excitons) are present in the current solar cell system at significant densities. In the FRM,[17-19] the description for each of these particles is associated with an event, and each event has a waiting time, τ_q. An event is associated with a configurational change in the system; for example, inserting or removing a particle or updating the coordinates of the particles. All the possible events in the system are stored in the order of ascending

waiting time and form a temporal sequence. This queue of events will constantly be updated to reflect the time evolution of the system. At each time step, the event at the start of the queue is selected to execute and then removed from the queue. Later on, the simulation time is incremented by the time expired and all of the waiting times in queue are reduced by this time expired. The execution of a current event will probably preclude the occurrence of subsequent events, in conformance with certain rules (e.g. the single occupancy of lattices), and in turn, it requires that the newly enabled event be created and then inserted in the queue. Marsh et al. have demonstrated that the dynamic properties of carriers can be indistinguishably described by both the FRM and the full dynamical Monte Carlo algorithm (in which the whole event queue must be updated for every configuration change).[10]

The waiting time τ_q is calculated as

$$\tau_q = -\frac{1}{W}\ln(X) \tag{3}$$

where X is a random number uniformly distributed in (0, 1) and W is the occurring rate of an event. For each particle, only the event that occurs first needs to be inserted in the queue. As a result, we need to calculate the waiting time for all the events available to a particular particle and select the event with the smallest waiting time as the event for the particle that is to be inserted to the event queue.

In our simulations, excitons are created at randomly chosen sites in either the hole or electron conducting polymer at constant rate. The time interval is the inverse of the exciton creation rate, $W_{eg} = 900$ s^{-1} nm^{-2} calculated from the AM1.5 solar spectrum with an illumination of 90 mW/cm^2 and the absorption spectrum (with wavelength below 800 nm, in consideration of the IPCE spectrum) of the polymer blend.[6] There are three events available to a freshly generated exciton: hopping, recombination, and dissociation at the interface. The excitons generated in these polymers are singlet ones in almost all cases prior to dissociation at the donor and acceptor interface. Therefore, the exciton dissociation rate, W_{ed}, must be set sufficiently high. In organic semiconductors, the exciton lifetime is about 500 ps, and the diffusion length of exciton is estimated to be around 10−20 nm[1] in these polymers. The given hopping rate from the current site, i, to a nearby site, j, is given by

$$W_{ij} = W_e\left(\frac{R_0}{R_{ij}}\right)^6 \begin{cases} \exp\left(-\dfrac{E_j - E_i}{k_B T}\right) & : \quad E_j > E_i \\ 1 & : \quad E_j \leq E_i \end{cases} \tag{4}$$

where R_{ij} is the distance between hopping sites i and j, R_0 is the exciton localization radius, W_e is the hopping attempt frequency, and E_i and E_j are the occupation energies of the two sites. As a first-order approximation, the site energy E_i for the exciton is set to zero because the exciton is a neutral particle; thus, eq 4 can be simplified as

$$W_{ij} = W_e\left(\frac{R_0}{R_{ij}}\right)^6 \tag{5}$$

Hopping rates for excitons are evaluated by including lattice neighbors out to a radius of 15 nm. The parameters $W_e R_0^6 = 2$ nm^6 ps^{-1} and exciton recombination rate $W_{er} = 1/500$ ps^{-1} are set to make sure that the excitons have a diffusion length of ~10 nm. In our model, the exciton hopping is allowed only between the same material sites. After hopping, excitons will be subject to a new enabled event selection process until they

eventually recombine or are dissociated at an interface between the electron and hole conductors.

Charge carriers (electrons and holes) can be imported into the system by the exciton dissociation or injection from the electrodes, and the electron (hole) can occupy only the electron (hole) conductor site. All electrostatic interactions in the device are included in the model, and the Coulombic interaction between sites i and j is calculated as

$$V_{ij} = \frac{q_i q_j}{4\pi\varepsilon_0\varepsilon}\frac{1}{R_{ij}} \tag{6}$$

where q_i and q_j are the site charges, respectively; ε is the dielectric constant; and R_{ij} is the distance between sites i and j.

Once created, the charge carriers must be assigned an event by selecting the most viable one (with the smallest waiting time) from the three possible events; that is, hopping, charge recombination, and extraction by the electrodes. The hopping rate of charge carriers is calculated using the Marcus theory,[20]

$$W_{ij} = V_{hop}\exp\left(-\frac{(E_j - E_i + E_r)^2}{4E_r k_B T}\right) \tag{7}$$

E_i and E_j are the energies of hopping sites i and j, respectively, and E_r corresponds to twice the polaronic binding energy.[10] For the charge carriers, all the Coulomb interactions between neighboring charges (within a distance less than R_c) and modifications from the effect of the internal electric field are included in calculating the site energy. Hopping is restricted to the adjacent sites (the nearest neighboring sites; thus, there are six adjacent sites in a cubic lattice), whose energy is calculated by taking into account the Gaussian standard deviation σ to the density of states. The prefactor, V_{hop}, is derived from the Einstein relationship under isoenergetic site condition as[9,10]

$$V_{hop} = \frac{6k_B T\mu_{e/h}}{qa_0^2}\exp\left(\frac{E_r}{4k_B T}\right) \tag{8}$$

where $\mu_{e/h}$ is the charge mobility and is chosen as 10^{-3} cm^2 V^{-1} s^{-1} for the blend of polymer type 1 and type 2. We also assume that electrons and holes have equal mobility in our simulations. Therefore, the V_{hop} is set as 1.06×10^{-2} ps^{-1}. If the electron and hole are located on the adjacent sites, they may recombine. As a result, the charges are lost, and we set the rate to $W_{cr} = 10^{-6}$ ps^{-1}.

Similarly, to study the charge injection process from electrodes, each appropriate electrode site (electron conductor at cathode or hole conductor at anode) is expected to inject a charge carrier at a time interval determined by its characteristic injection rate. This process is also treated as a hopping event from the Fermi level of electrode material to the adjacent polymer site and then integrated into the FRM algorithm. The injection rate is calculated using the same Marcus formula (eq 7), and the difference in the mean value of the involved site energies (E_j and E_i) equals the energy barrier (E_{IB}) of 0.4 eV (the difference between the LUMO of polymer type 1 and the Fermi level of Al). The Gaussian disorder for the density of states is also taken into account in calculating the site energy for charge injection. As a result, the difference between the involved site energies E_j and E_i is the sum of the energy barrier (E_{IB}) and the contribution from Gaussian disorder for the density of states. A charge carrier adjacent to an electrode is extracted from the device with a designated rate W_{ce}. We treat this extraction as an inverse process of charge injection, and then W_{ce} is calculated. To simulate the effect of "charge leak", the electron (hole) can be extracted from the device at both the

MC Simulation for Polymer Blend Photovoltaics

J. Phys. Chem. B, Vol. 114, No. 1, 2010 **39**

TABLE 1: Parameters Used in the Modeling[a]

T	298.0 K	temperature
ε	3.5	dielectric constant
a_0	3 nm	lattice constant
R_c	15 nm	cutoff distance
W_{eg}	900 s^{-1} nm^{-2}	exciton creation rate
$W_e R_0^6$	2 nm^6 ps^{-1}	exciton hopping rate
W_{er}	2×10^{-3} ps^{-1}	exciton recombination rate
E_r^*	0.187 eV	twice the polaronic binding energy
V_{hop}	1.06×10^{-2} ps^{-1}	charge hopping rate
σ^*	0.062 eV	Gaussian standard deviation
W_{cr}	1×10^{-6} ps^{-1}	charge recombination rate
$\Delta\Phi$	0.5 V	difference in work functions of electrodes
E_{IB}	0.4 eV	energy barrier for charge injection

^{a} The parameters with * are taken from ref. 10. The charge recombination rate is in consideration of the corresponding parameter set in ref. 10.
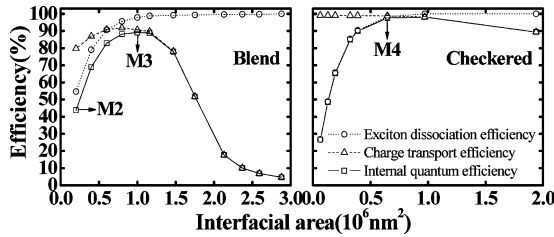

Figure 4. For the blend and checkered morphologies, the exciton dissociation efficiency, the charge collection efficiency, and the internal quantum efficiency vary with interfacial area between the electron and the hole conductors.

Figure 5. The modeled $I-V$ performance curves for the M3 and M4 compared with experiment results[6] under similar conditions.

TABLE 2: The Key Simulation Results for Different Morphologies Compared with the Experimental Values

morphology	I_{SC} (mA/cm^2)	V_{OC} (V)	ff	P_{OP} (mW/cm^2)	PCE (%)
M3	10.28	0.50	0.390	2.006	2.229
M4	11.99	0.50	0.409	2.453	2.726
experiment[6] (100 mW cm^{-2})	4.195	0.63	0.386	1.019	>1

TABLE 3: Short-Circuit Current and Open-Circuit Voltage for Bilayer Morphology M1 under Different Light Intensities

intensity (sun)	I_{SC} (mA/cm^2)	V_{OC} (V)
0.1	0.215	0.91
1.0	2.149	1.00
10	21.50	1.07

cathode and anode. These treatments for charge injection and extraction can lead to a typical charge density ($\sim 10^{22}$ m^{-3}) in our models, which is also close to the experimental value. The image charge effects are also included in calculating the Coulombic interactions for charges near the electrodes (up to the cutoff radius).[12-14] This modification ensures that the potential at each electrode be fixed because the dark current injection is involved in the simulations. Finally, the destination of charges is either the extraction from electrodes or the recombination with an opposite charge in the system. The built-in field under short circuit conditions arises from the difference between the work functions of the Al cathode and the ITO anode ($\Delta\Phi = 0.5$ V). All parameters used in the Monte Carlo simulation are listed in Table 1.

After reaching a steady state, the IQE and the current density for different conditions are saved and calculated over a time interval long enough to average out the fluctuations (typically >0.1 s). Under the current assumption, the parameters will not change with the scale of phase separation.[9,10] The charge extracted from the electrodes per area and unit time is taken as the current density. Then, the outside circle current is calculated as the average of the net current density at the cathode and anode, respectively.

3. Results and Discussion

Under the short-circuit conditions, the IQE and its two constituent components, the exciton dissociation efficiency (the ratio of the number of excitons dissociated to the number of excitons generated) and charge collection efficiency (the ratio of the net number of charges that exit the device to twice of the number of excitons dissociated), are calculated for various blends and checkered morphologies and are plotted as shown in Figure 4. Generally, the exciton dissociation tends to increase, whereas the charge collection efficiency will decrease as the
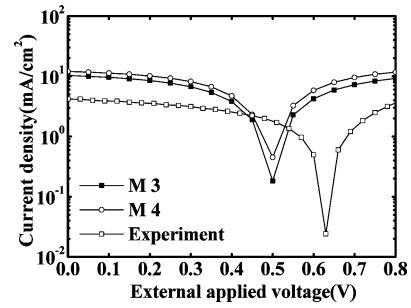
interfacial area increases. By balancing these two competitive component efficiencies, two optimal morphologies are obtained, as shown in Figure 3 (M3 for the blend series and M4 for the checkered series). These two cases lead to the peak IQE and are chosen as the bases for analyzing the $I-V$ performance. For the blend series, the peak IQE corresponds to the characteristic feature size of around 10 nm, whereas for the checked series, the maximum IQE occurs when the width of the square rods is around 9 nm. Detailed analysis shows that, for the blend morphologies with low interfacial area (e.g., the M2), the pure phases are not perfectly separated due to the thermal effect in the Ising model and, thus, many small isolated islands remain in those majority phases. These islands tend to act as traps for the free charges that can only be gotten rid of by waiting for the opposite charges to recombine at the interface between the islands and the majority phases. As a result, the charge collection efficiency for the M2 can not reach the 100% level as expected, but a peak can occur at a large-scale phase separation.[9]

The performance for the optimal morphologies offers a good guidance to show how much experimental work needs to be done. Figure 5 shows the $I-V$ performance of the optimal morphologies using the parameters listed in Table 1. Our calculations can reproduce the important features in the experimental work, which are described in Table 2. The fill factor calculated is around 0.4 and is in good agreement with experimental result. The open circuit in the blend and checkered morphologies corresponds approximately to the flat-band condition (the internal electric field equals 0);[10,21] thus, the open-circuit voltage in our simulations is equal to the difference in work functions of the electrodes in these two cases. In addition, all processes involved in our models are symmetrical along the electrode direction in these two cases. The expected optimal power conversion efficiency (PCE) can reach as high as 2.2% for the blend polymer (see Table 2).

For the bilayer morphology (M1), the extra contribution to V_{OC} increases with intensity, which is in accordance with the
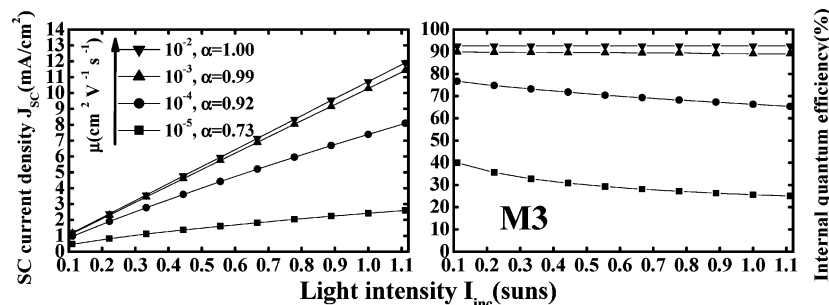
Figure 6. The dependency of short-circuit current and internal quantum efficiency on the mobility and the light intensity for the morphology M3. J_{SC} is related to I_{inc} as $J_{SC} \propto I_{inc}{}^\alpha$, and α varies with mobility.

experimental work. The origin of this extra contribution in bilayer morphology is speculated to be charge-density-gradient-related. The magnitude of this increase, 0.07−0.09 V/decade, as shown in Table 3, is consistent with the work by Marsh et al.,[10] and the theoretical prediction (0.06 V/decade) based on the superposition of dark and light current by Barker et al.[22]

The model can also be used to investigate the effects of some other physical quantities of interest to experimentalists, such as exciton creation rate, exciton diffusion length, charge mobility, and charge recombination rate on the short-circuit current and IQE. As shown in Figure 6, the short-circuit current increases sublinearly with increasing light intensity or exciton creation rate. However, when the charge mobility is over 10^{-3} cm^2 V^{-1} s^{-1}, the short-circuit current and the internal quantum efficiency are not sensitive to the mobility, and as a result, a further increase in mobility does not significantly improve the device's performance. This means that as a way to improve the PCE, the strong absorption is more effective than the high mobility, especially because the particular mobility is high enough to extract almost all the charges diffusing in the system.

A typical feature of organic solar cells is that the short-circuit current density, J_{SC}, does not scale linearly with the exciton generation rate, W_{eg}, or light intensity, I_{inc}.[23] Instead, a power law relationship is found and given by $J_{SC} \propto I_{inc}{}^\alpha$, where $\alpha \le 1$.[24,25] This deviation from linearity ($\alpha = 1$) is speculated to arise from the occurrence of nongeminate charge recombination.[10,23,25] In our simulations, we have assumed that the electrons and holes have equal mobility. It should be emphasized here that the current model is correct only for the balanced electron and hole mobilities, and this situation facilitates derivation of the maximum efficiency conditions. However, if the mobilities for electron and hole are different, it will leads to space−charge accumulation, which tends to limit the photocurrent at high intensity.[10,24] When the charge mobility decreases, the average time for free charges exiting from the device tends to increase, and the occurrence probability of nongeminate charge recombination would increase. These result in a bigger deviation from unity for α and a more rapid decrease in IQE with increasing light intensity, as shown in Figure 6.

The effects of exciton diffusion length and charge recombination rate on the IQE are also studied and are shown in Figures 7 and 8, respectively. As the exciton diffusion length increases, the exciton dissociation efficiency tends to increase, and this leads to an increase in the IQE, especially for the coarse-blend morphologies, as shown in Figure 7. The IQE peak will be shifted toward the coarser-blend morphologies with increasing exciton diffusion length, as desired.

As shown in Figure 8, the exciton dissociation rate remains unaffected as the charge recombination rate changes. This is a reasonable result because the particle density in a organic solar cell (including exciton and charge carriers) is low enough that
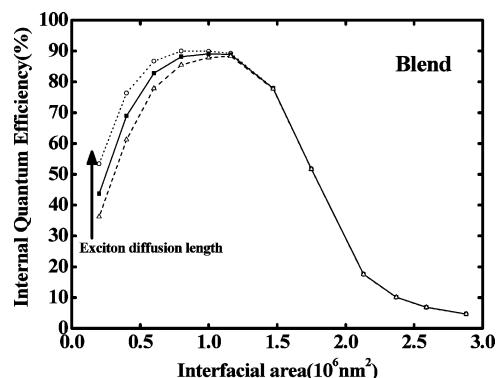

Figure 7. The dependency of internal quantum efficiency on the exciton diffusion length for the morphology M3. The corresponding exciton diffusion lengths in simulations are 7 ($\triangle$), 10 ($\square$), and 15 nm ($\bigcirc$).
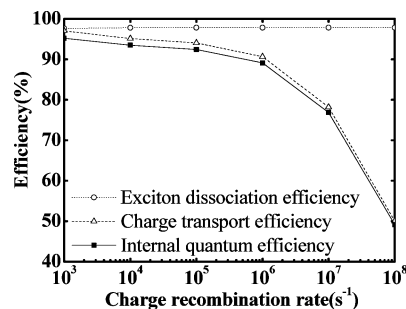

Figure 8. The dependency of internal quantum efficiency on the charge recombination rate for the morphology M3.

the behavior of the exciton will not be disturbed by the movement of charge carriers and vice versa. This conclusion is also confirmed for a variety of charge mobilities (10^{-5}−10^{-2} cm^2 V^{-1} s^{-1}). However, as the charge recombination rate increases, the charge transport rate and then the IQE tend to decrease due to the more frequent occurrence of nongeminate charge recombination. The short-circuit current changes in the same way as the IQE does. In calculating the PCEs for the M3 and the M4, we set the charge recombination rate as 10^{-6} ps^{-1}.

In addition to these important physical quantities closely related to experiments, some other parameters introduced in our MC model (such as lattice constant) can also be of interest. It is demonstrated that the qualitative conclusions discussed here will not be affected by varying the lattice constant, and they are also consistent with the previous simulations.[10] In addition, some more subtle descriptions (such as the fluctuation of lattice constant) and other mechanisms governing these key processes in solar cells can also be incorporated in the FRM to further improve the model.

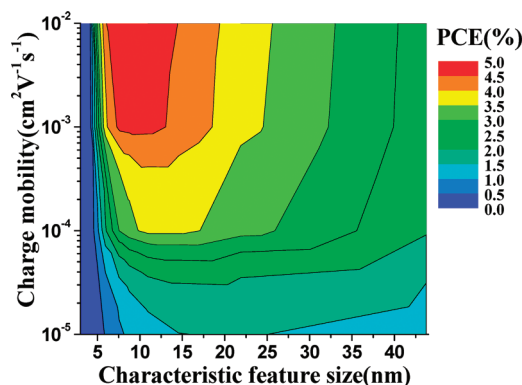Recent theoretical calculations based on analysis of energy levels of frontier orbits have predicted that a 10% power

MC Simulation for Polymer Blend Photovoltaics

J. Phys. Chem. B, Vol. 114, No. 1, 2010 **41**

Figure 9. Contour plots showing the calculated power conversion efficiency (PCE) for the blend morphologies versus the charge mobility and the characteristic feature size in the blend. The V_{OC} and the fill factor used in the calculation are 0.63 V and 0.65, respectively.

conversion efficiency for a polymer/fullerene system is possible,[26] and the PCE can even approach 15% by resorting to the tandem solar cell.[27] In our model, the quantum effect leading to a bigger V_{OC} cannot be reflected, and the open-circuit voltage for the M3 and the M4 in our simulations is roughly equal to the difference in work functions of the electrodes (0.5 V). When an experimental value of 0.63 V for the V_{OC} and a value of 0.65[26] for the fill factor are chosen, the PCE contour curves for the blend morphologies are plotted in Figure 9, and a limiting 5% PCE can be approached, as shown in the figure.

As is well-known, the PCE is mostly sensitive to the polymer nanostructure, light absorption, and charge mobility. An ideal domain size in morphology (~10 nm)[28] or adoption of specialized structure (e.g., the checkered[1] or the gyroidal morphology,[29]) are the key factors for increasing the PCE. Except for the morphological aspects, some inevitable effects in experiment (for example, the impurity in materials, mirror loss of absorption at the electrode, and the traps for charges, etc.) could also lead to a decrease in the experimental PCE or the short-circuit current density, which is clearly in action in our simulation.

4. Conclusion

To conclude, we have carried out a comprehensive dynamic Monte Carlo simulation, including the exciton creation and the diffusion and the dark and light current mechanism, to simulate the performance of an organic solar cell made purely of polymers. The parameters are basically chosen from the experimental measurements of the novel polymer blend, which features strong absorption. Under the short circuit condition, the optimal morphologies with peak IQE can be generated by using the Ising model and are chosen through the IQE calculations. A power conversion efficiency of around 2.2% can be achieved, which is higher than the experimental value (>1%). An even higher PCE (~5%) can be expected for optimal charge mobility combined with optimal film morphology. These convince us that there still exists much room for improvement in the experimental aspects.

To further explore the polymer systems, we extend our parameters to go beyond the typical range. Some experimental features—for example, the extra contribution to V_{OC} for the

bilayer morphology and the sublinearity dependency of J_{SC} on light intensity—can be quantitatively described by our model. By comparing the effects of charge mobility and exciton creation rate on the short-circuit current, we have found that improving the absorption of polymer materials coupled with effective exciton dissociation is the most effective way for increasing the PCE of an organic solar cell. Finally, the complicated dependency of the PCE on the charge mobility and material morphology can also be described by our model.

References and Notes

(1) Gunes, S.; Neugebauer, H.; Sariciftci, N. S. *Chem. Rev.* **2007**, *107*, 1324.
(2) Sariciftci, N. S.; Braun, D.; Zhang, C.; Srdanov, V. I.; Heeger, A. J.; Stucky, G.; Wudl, F. *Appl. Phys. Lett.* **1993**, *62*, 585.
(3) Yu, G.; Gao, J.; Hummelen, J. C.; Wudl, F.; Heeger, A. J. *Science* **1995**, *270*, 1789.
(4) Granstrom, M.; Petritsch, K.; Arias, A. C.; Lux, A.; Andersson, M. R.; Friend, R. H. *Nature* **1998**, *395*, 257.
(5) Kietzke, T.; Horhold, H.-H.; Neher, D. *Chem. Mater.* **2005**, *17*, 6532.
(6) Zhan, X.; Tan, Z. a.; Domercq, B.; An, Z.; Zhang, X.; Barlow, S.; Li, Y.; Zhu, D.; Kippelen, B.; Marder, S. R. *J. Am. Chem. Soc.* **2007**, *129*, 7246.
(7) Hou, J.; Tan, Z. a.; Yan, Y.; He, Y.; Yang, C.; Li, Y. *J. Am. Chem. Soc.* **2006**, *128*, 4911.
(8) Koster, L. J. A.; Smits, E. C. P.; Mihailetchi, V. D.; Blom, P. W. M. *Phys. Rev. B* **2005**, *72*, 085205.
(9) Watkins, P. K.; Walker, A. B.; Verschoor, G. L. B. *Nano Lett.* **2005**, *5*, 1814.
(10) Marsh, R. A.; Groves, C.; Greenham, N. C. *J. Appl. Phys.* **2007**, *101*, 083509.
(11) Scott, J. C.; Malliaras, G. G. *Chem. Phys. Lett.* **1999**, *299*, 115.
(12) Wolf, U.; Arkhipov, V. I.; Bässler, H. *Phys. Rev. B* **1999**, *59*, 7507.
(13) Arkhipov, V. I.; Wolf, U.; Bässler, H. *Phys. Rev. B* **1999**, *59*, 7514.
(14) Barth, S.; Wolf, U.; Bässler, H. *Phys. Rev. B* **1999**, *60*, 8791.
(15) Hou, J.; Yang, C.; He, C.; Li, Y. *Chem. Commun.* **2006**, 871.
(16) Sun, S.-S. *Sol. Energy Mater. Sol. Cells* **2003**, *79*, 257.
(17) Gillespie, D. T. *J. Comput. Phys.* **1976**, *22*, 403.
(18) Jansen, A. P. J. *Comput. Phys. Commun.* **1995**, *86*, 1.
(19) Lukkien, J. J.; Segers, J. P. L.; Hilbers, P. A. J.; Gelten, R. J.; Jansen, A. P. J. *Phys. Rev. E* **1998**, *58*, 2598.
(20) Marcus, R. A. *Rev. Mod. Phys.* **1993**, *65*, 599.
(21) Moliton, A.; Nunzi, J.-M. *Polym. Int.* **2006**, *55*, 583.
(22) Barker, J. A.; Ramsdale, C. M.; Greenham, N. C. *Phys. Rev. B* **2003**, *67*, 075205.
(23) Riedel, I.; Martin, N.; Giacalone, F.; Segura, J. L.; Chirvase, D.; Parisi, J.; Dyakonov, V. *Thin Solid Films* **2004**, *451*−*452*, 43.
(24) Koster, L. J. A.; Mihailetchi, V. D.; Xie, H.; Blom, P. W. M. *Appl. Phys. Lett.* **2005**, *87*, 203502.
(25) Gebeyehu, D.; Pfeiffer, M.; Maennig, B.; Drechsel, J.; Werner, A.; Leo, K. *Thin Solid Films* **2004**, *451*, 29−452.
(26) Scharber, M. C.; Mühlbacher, D.; Koppe, M.; Denk, P.; Waldauf, C.; Heeger, A. J.; Brabec, C. J. *Adv. Mater.* **2006**, *18*, 789.
(27) Dennler, G.; Scharber, M. C.; Ameri, T.; Denk, P.; Forberich, K.; Waldauf, C.; Brabec, C. J. *Adv. Mater.* **2008**, *20*, 579.
(28) Moon, J. S.; Lee, J. K.; Cho, S.; Byun, J.; Heeger, A. J. *Nano Lett.* **2009**, *9*, 230.
(29) Crossland, E. J. W.; Kamperman, M.; Nedelcu, M.; Ducati, C.; Wiesner, U.; Smilgies, D.-M.; Toombes, G. E. S.; Hillmyer, M. A.; Ludwigs, S.; Steiner, O. U.; Snaith, H. J. *Nano Lett.* **2009**, *9*, 2807.